Geosci. Model Dev. Discuss., 7, 1671–1707, 2014
www.geosci-model-dev-discuss.net/7/1671/2014/
doi:10.5194/gmdd-7-1671-2014
© Author(s) 2014. CC Attribution 3.0 License.

Geoscientific Model Development Discussions
Open Access

This discussion paper is/has been under review for the journal Geoscientific Model Development (GMD). Please refer to the corresponding final paper in GMD if available.

# Implementation of a soil albedo scheme in the CABLEv1.4b land surface model and evaluation against MODIS estimates over Australia

**J. Kala[1], J. P. Evans[1], A. J. Pitman[1], C. B. Schaaf[2], M. Decker[1], C. Carouge[1], D. Mocko[3], and Q. Sun[2]**

[1]Australian Research Council Centre of Excellence for Climate Systems Science and Climate Change Research Centre, University of New South Wales, Sydney, NSW, 2052, Australia
[3]SAIC at NASA Goddard Space Flight Centre, NASA, Greenbelt, MD, USA
[2]Department of Earth and the Environment, Boston University, Boston, Massachusetts, USA

Received: 23 January 2014 – Accepted: 5 March 2014 – Published: 13 March 2014

Correspondence to: J. Kala (j.kala@unsw.edu.au, jatin.kala.jk@gmail.com)

Published by Copernicus Publications on behalf of the European Geosciences Union.







## Abstract

Land surface albedo, the fraction of incoming solar radiation reflected by the land surface, is a key component of the earth system. This study evaluates snow-free surface albedo simulations by the Community Atmosphere Biosphere Land Exchange (CABLEv1.4b) model with the Moderate Resolution Imaging Spectroradiometer (MODIS) albedo. We compare results from two offline simulations over the Australian continent, one with prescribed background snow-free and vegetation-free soil albedo derived from MODIS (the control), and the other with a simple parameterisation based on soil moisture and colour. The control simulation shows that CABLE simulates albedo over Australia reasonably well, with differences with MODIS within an acceptable range. Inclusion of the parameterisation for soil albedo however introduced large errors for the near infra red albedo, especially for desert regions of central Australia. These large errors were not fully explained by errors in soil moisture or parameter uncertainties, but are similar to errors in albedo in other land surface models which use the same soil albedo scheme. Although this new parameterisation has introduced larger errors as compared to prescribing soil albedo, dynamic soil moisture-albedo feedbacks are now enabled in CABLE. Future directions for albedo parameterisations development in CABLE are discussed.

## 1 Introduction

The albedo of the land surface is the ratio of upwelling to downwelling shortwave radiation and determines the fraction of incoming solar radiation reflected back to the atmosphere. It is one of the key drivers of the earth's climate as it determines, in part, the amount of energy available to drive processes in the atmosphere and the land surface (e.g., Dickinson, 1983). Hence, the incorrect prescription or parameterisation of surface albedo can result in large model biases. Therefore, the correct representation





GMDD
7, 1671–1707, 2014



of albedo in land surface models (LSMs), whether prescribed or parameterised, is of critical importance to the surface energy and hydrological cycle.

The overall albedo of the land is a function of the vegetation, soil, and snow albedos. The main factor which determines which of these three albedos has the strongest influence on the overall surface albedo is the fractional area covered by each of vegetation, soil and snow. These are commonly parameterised as a function of leaf area index (LAI), the total one-sided surface area of leaf per ground surface area (Bonan, 2008). When LAI is high, most of the incoming solar energy is reflected, scattered, and/or absorbed by the vegetation canopy and only a small proportion of radiation reaches the ground and the overall albedo is primarily that of the vegetation canopy. When LAI is small, the converse is true and the overall albedo is primarily that of the soil or snow.

Vegetation albedo is a function of the radiative properties of the canopy, i.e., the leaf transmittance and reflectance, as well its physical properties, namely, the leaf angle or orientation, canopy clumping and structure. Leaf transmittance and reflective properties determine how much radiation penetrates through the canopy and are usually prescribed in LSMs for each plant functional type (PFT) in the visible (VIS, 0.4–0.7 µm) and near infra-red (NIR, 0.7–4.0 µm) bands. This distinction is important since green canopies absorb most of the solar radiation in the VIS waveband for photosynthesis, but reflect and transmit most of the radiation in the NIR waveband (Bonan, 2008). Leaf structural and physical properties can also influence within-canopy shadowing, which allows higher exposure of the underlying soil and/or snow cover, especially in low density forests (Davidson and Wang, 2004). Leaf orientation influences albedo since the maximum incident solar radiation on a leaf occurs when the beam is perpendicular to the surface (Bonan, 2008).

Soil albedo is a function of soil colour, determined partly by its organic composition, and more importantly, soil moisture, with saturated soils generally having lower albedo than dry soils (Idso et al., 1975). This is especially important in transitional climatic regions, where significant soil moisture variability drives strong land–atmosphere coupling (e.g., Koster et al., 2004). Although the dependence of soil albedo on soil moisture





GMDD
7, 1671–1707, 2014



has been well established from field experiments (e.g., Idso et al., 1975), several LSMs do not include this feedback and recent studies have shown that it plays in important role in seasonal droughts in the central US (Zaitchik et al., 2012). Recent studies over eastern Australia have shown that the use of time-varying MODIS albedo as opposed to monthly mean climatologies from AVHRR in a regional climate model improved mean air temperature simulations, and to a lesser extent, precipitation (Meng et al., 2013). This was particularly evident in arid regions, where the overall albedo is predominantly influenced by soil rather than vegetation.

Vegetation and soil albedo are also influenced by the solar zenith angle, especially in desert regions (Wang et al., 2005). This only applies under clear-sky conditions (i.e., direct beam radiation) when there is little or no scattering of the incoming shortwave radiation. In the morning just after sunrise and late afternoon before sunset, albedo is generally higher, as compared to mid-day when the sun is directly overhead. The inclusion of soil and vegetation albedo dependence on solar zenith angle during clear-sky conditions has improved albedo simulations in some LSMs (Liang et al., 2005).

With recent developments in satellite remote sensing, several surface albedo products are now available at a high spatial and temporal resolution and spanning several years. This has allowed for the careful evaluation of albedo in various LSMs (e.g., Wei et al., 2001; Oleson et al., 2003; Zhou et al., 2003; Wang et al., 2004); the development of vegetation and soil albedo parameterisations (e.g., Liang et al., 2005; Yang et al., 2008); as well as the mapping of land surface parameters such as the spatial and temporal distribution of PFTs, LAI and soil color, for use in LSMs (Lawrence and Chase, 2007). Clearly, the use of satellite remote sensing can be very useful in both the evaluation and development of LSMs.

This paper focusses on the Community Atmosphere Biosphere Land Exchange (CABLE) model (Wang et al., 2011), an LSM designed to simulate fluxes of heat, moisture, and carbon at the land surface. While several studies have used CABLE (e.g., Cruz et al., 2010; Zhang et al., 2011; Pitman et al., 2011; Wang et al., 2012; Exbrayat et al., 2012), no studies have explicitly examined simulations of surface albedo. The aim of





GMDD
7, 1671–1707, 2014



this paper is to address this key knowledge gap by comparing CABLE albedo simulations with MODIS albedo to better quantify the errors in CABLE albedo simulations. Section 2 provides on overview of CABLE with detailed description of the parameterisation of surface albedo. This is followed by the experimental design and description of the satellite remote sensing products used to compare against CABLE albedo simulations. Results are presented in Sect. 3 and discussed in Sect. 4.

## 2 Methods

### 2.1 Model description

CABLE simulates fluxes of energy, water and carbon at the land surface and can be run as an offline-model with prescribed meteorology (e.g., Abramowitz et al., 2008; Wang et al., 2011; Kala et al., 2013) or fully coupled to an atmospheric model within a global (Mao et al., 2011) or regional atmospheric model (Hirsch et al., 2013). CABLE is a key part of the Australian Community Climate Earth System Simulator (ACCESS, see http://www.accessimulator.org.au), a fully coupled earth system science model, currently being used as part of the Coupled Model Intercomparison Project Phase 5 (CMIP-5). The version used in this study is CABLEv1.4b.

In CABLEv1.4b (Wang et al., 2011), the one-layered, two-leaf canopy radiation module of Wang and Leuning (1998) is used for sunlit and shaded leaves and the canopy micro-meteorology module of Raupach (1994) is used for computing surface roughness length, zero-plane displacement height, and aerodynamic resistance. The model also consists of a surface flux module to compute the sensible and latent heat flux from the canopy and soil, the ground heat flux, as well as net photosynthesis. A soil module is used for the transfer of heat and water within the soil and snow, and an ecosystem carbon module based on Dickinson et al. (1998) is used for the terrestrial carbon cycle. A detailed description of each of the modules can be found in Kowalczyk et al. (2006) and Wang et al. (2011).





GMDD
7, 1671–1707, 2014





Albedo in CABLE is a function of the vegetation albedo, snow albedo, and the background snow-free and vegetation-free soil albedo. The parameterisation of albedo is part of the canopy radiative transfer model. The latter accounts for direct beam and diffuse radiation separately, and within each stream, albedo is computed separately in the NIR and VIS wavebands as plants utilise energy differently in these two parts of the spectrum. Appendix A provides a detailed description of the albedo parameterisation and a schematic illustration is presented in Fig. 1.

The overall albedo of the surface (snow-free) is a function of the direct and diffuse effective reflectances and the fraction of direct beam shortwave radiation in the NIR and VIS wavebands (see Eq. A1 and Fig. 1). When running CABLE offline, the fraction of direct beam shortwave radiation is computed empirically from incoming shortwave radiation (meteorological input to the model), solar constant, julian day of year, and solar zenith angle, following Spitters (1986). When coupled, it is provided by the atmospheric radiation model. The direct and diffuse effective reflectances are a function of the canopy reflectance and extinction coefficients for direct and diffuse radiation, the soil reflectance, and LAI (see Eqs. A2 and A3 and Fig. 1). In CABLEv1.4b, LAI is prescribed as the model does not include a dynamic vegetation model or dynamic phenology, and the soil reflectance is derived from the background snow and vegetation-free soil albedo, which is also prescribed.

The canopy reflectance for direct radiation is a function of the direct and diffuse extinction coefficients for a black canopy and the reflectance of a homogenous canopy with horizontal black leaves (see Eq. A4). The canopy reflectance for diffuse radiation is in turn dependant on the canopy reflectance for direct radiation, and the solar zenith angle (see Eq. A5). The extinction coefficients for direct and diffuse radiation are a function of the corresponding extinction coefficients for a black canopy, and the leaf transmittance and reflectance (see Eq. A6). The direct and diffuse extinction coefficients for a black canopy are a function of solar zenith angle, LAI, and leaf angle (see Eqs. A7–A11). Finally, the reflectance of a horizontal homogeneous canopy with horizontal black leaves is also a function of the leaf radiative properties (see Eq. A12). In





GMDD
7, 1671–1707, 2014



summary, the albedo parameterisation in CABLE is reasonably complex, as illustrated in Fig. 1. User-defined input parameters which influence albedo are the LAI, background snow and vegetation-free soil albedo, leaf angle, and the leaf transmittance and reflectance.

While it is common to prescribe LAI and leaf physical and radiative properties in most LSMs, several LSMs include simple parameterisations for the background snow and vegetation-free soil albedo based on soil moisture content. Since this soil moisture-albedo feedback has been shown to be important (e.g., Vamborg et al., 2011; Zaitchik et al., 2012), we added a simple parameterisation based on soil colour and moisture, originally developed for the Biosphere–Atmosphere Transfer Scheme (BATS) LSM (Dickinson et al., 1993), and adopted by the Common Land Model (CLMv2.0) (Zeng et al., 2002):

$$\Delta = \max(0.11 - 0.40\theta_{sm}, 0) \quad (1)$$

$$\alpha_{soil} = \min(\alpha_{sat} + \Delta, \alpha_{dry}) \quad (2)$$

where $\alpha_{sat}$ and $\alpha_{dry}$ are the albedo of saturated and dry soils respectively, dependant on the soil colour (light to dark), as shown in Table 2, and $\theta_{sm}$ is the surface volumetric soil moisture content.

We note that the saturated and dry soil albedos in the VIS waveband as shown in Table 2 are simply assumed to be twice those in the NIR waveband. As noted by Wang et al. (2004), this assumption is not un-reasonable, but other studies have shown this ratio varies geographically (Tsvetsinskaya et al., 2002).

### 2.2 Simulations

CABLEv1.4b was used within the NASA Land Information System (LIS-6.1) (Kumar et al., 2006, 2008), a flexible software platform designed as a land surface modelling and hydrological data assimilation system. A grid resolution of 0.25°×0.25° was utilised, covering continental Australia as illustrated in Fig. 2a, showing the distribution of PFTs.





GMDD
7, 1671–1707, 2014



The model was forced with the Modern Era Retrospective-analysis for Research and Applications (MERRA) reanalysis (Rienecker et al., 2011) at 3 hourly intervals from 2001–2008 and initialised from a previous 30-year spin-up. This year range was chosen as it corresponded with the availability of the remotely sensed albedo products. The forcing variables included incoming long-wave and shortwave radiation, air temperature, specific humidity, surface pressure, wind speed and precipitation. The MERRA reanalysis was bias-corrected for precipitation using the Australian Bureau of Meteorology Australian Water Availability gridded precipitation dataset (Jones et al., 2009), following Decker et al. (2012). A monthly mean MODIS derived LAI climatology from Yuan et al. (2011) was used for the simulations as shown in Fig. 3. Although monthly mean values are used in the simulations, we show seasonal means in Fig. 3 to help the interpretation of seasonal differences in albedo in Sect. 3. Monthly ambient carbon dioxide concentrations were prescribed using measurements from Baring Head, New Zealand (Keeling et al., 2005). Outputs were saved every hour, for the direct and combined (direct and diffuse) albedos, in the VIS and NIR wavebands respectively.

As discussed in Sect. 2.1, in CABLEv1.4b, the background snow-free and vegetation-free soil albedo has to be prescribed by default. We used the MODIS derived vegetation and snow-free background soil albedo data from Houldcroft et al. (2009), shown in Fig. 2b. In this data-set, bare soil regions, as defined by the IGBP land-use classification map (used in CABLE), are assigned the mean albedo over the data period (October 2002 to December 2006), while partially vegetated pixels are assigned a soil albedo derived from a linear relationship between albedo and the Normalised Difference Vegetation Index (NDVI). A linear regression model is then used to estimate the background soil albedo corresponding to zero LAI (Houldcroft et al., 2009). This simulation was the control (CNTL) experiment. An additional simulation was also carried out with the background snow and vegetation-free albedo parameterised as per Eq. (2), hereafter referred to as experiment PSALB (where PSALB is referring to Parametrized (P) Soil (S) Albedo (ALB)). The spatial distribution of soil colours for the PSALB experiment is shown in Fig. 2c. For both the CNTL and PSALB simulations,





GMDD
7, 1671–1707, 2014



leaf transmittance and reflectance properties and leaf angles were prescribed for each PFT following previous studies using CABLE (Pitman et al., 2011; Avila et al., 2012). Sample model namelist files for the CNTL and PSALB experiments are available online at: https://bitbucket.org/jkala/gmd-2014-9/src.

### 2.3 MODIS albedo

The albedo products from MODIS have been extensively used for the purpose of evaluating albedo from various LSMs (Oleson et al., 2003; Zhou et al., 2003; Wang et al., 2004). In this study, we used the MODIS MCD43GF 30 arc-seconds gap-filled snow-free albedo product (available at: http://www.umb.edu/spectralmass/terra_aqua_modis/modis_brdf_albedo_cmg_gap_filled_snow_free_product_mcd43gf_v005). The MCD43D product utilizes directional reflectances from both the Aqua and Terra MODIS instruments to retrieve an appropriate surface anisotropy model and thus intrinsic measures of surface albedo (Lucht et al., 2000; Schaaf et al., 2002; Wang et al., 2004). The MCD43 product is validated to stage-3 signifying that the high quality retrievals are within 5 % of field measures. Additionally, a very recent field evaluation of the MCD43A product (from which the MCD43D is derived) found root mean square errors of less than 0.03 over over agricultural and grassland sites, and less than 0.02 over forested sites, during dormant snow-free periods (Wang et al., 2014). Therefore to be conservative, we only show differences between MODIS and simulated albedoes which are greater than 0.05. The MCD43D product also provides data quality flags for each grid cell, and approximately 75 % of grid-cells over the domain of interest were classified as high-quality (flags 0 and 1), and 25 % were temporally fitted (flag 2). These temporally fitted points were mostly confined north of 20° S, i.e., the northern tropical regions where cloud fraction is generally high.

To enable comparison with the simulations, the MODIS albedo products were interpolated to the grid domain used for the simulations. Following previous studies (Oleson et al., 2003; Zhou et al., 2003; Wang et al., 2004), we compared the CABLE simulated direct beam VIS and NIR albedos at local solar noon (obtained by combining





GMDD
7, 1671–1707, 2014



the appropriate longitude bands from hourly outputs), to the VIS and NIR black-sky albedos from MODIS. The MCD43 product retrieval is attempted every 8 days over 16 days of potential input. We computed means of the local solar noon direct VIS and NIR direct-beam albedos from CABLE over the same time-interval of data availability to enable more meaningful comparisons. The CABLE combined (direct and diffuse) VIS and NIR albedos were compared against the MODIS blue-sky VIS and NIR albedos. The MODIS blue-sky albedo represents both the diffuse and direct radiation and uses MODIS aerosol optical depth (the MOD04 product) where available or 0.2 as a mean climatology where unavailable. The blue sky-albedo used here is also valid at local solar noon, and hence is compared with the CABLE combined VIS and NIR albedos at the same time.

### 2.4 FLUXNET observations

While comparisons with MODIS albedo provide valuable information on CABLE's ability to simulate albedo, the correct partitioning of the available net radiation into sensible and latent heat fluxes is equally important. We therefore compare our simulations with available quality controlled and gap-filled FLUXNET flux-tower observations at the Tumbarumba and Howard Springs sites shown in Fig. 2b. Data from these sites have been previously used to evaluate LSMs over Australia (Abramowitz et al., 2008; Haverd et al., 2013).

### 2.5 AMSR-E soil moisture

Given the dependance of the new soil albedo parameterisation on soil moisture, it is useful to quantify the uncertainties in the simulated soil moisture. Given the lack of in-situ soil moisture observations, we used satellite derived soil moisture from the Advanced Microwave Scanning Radiometer-Earth Observing System (AMSR-E), which uses brightness temperatures to derive surface soil moisture. The version of the AMSR-E data used in this study is described in Liu et al. (2009).





GMDD
7, 1671–1707, 2014



## 3 Results

Figures 4 and 5 show the yearly and seasonal differences between CABLE and MODIS white-sky and black-sky NIR and VIS albedo for the CNTL and PSALB experiments respectively (i.e., CNTL-MODIS and PSALB-MODIS respectively) and biases and root-mean-square-errors (RMSE) are shown in Table 3 (the RMSE and bias values are scaled by 100 such that small differences are easier to see). The CNTL experiment (with prescribed soil albedo), shows that CABLE simulates albedo well (Fig. 4). The model has a systematic under-estimation of the Black-Sky NIR albedo, especially during DJF (summer) of around 0.1 and over-estimation of the Blue-Sky VIS albedo for all seasons between 0.05 and 0.1. This over-estimation of Blue-Sky VIS albedo is over most of the interior continent, which has low LAI (Fig. 3). This suggests that part of this bias may be inherited from the prescribed soil albedo used (Fig. 2b), however, the bias is also present in the northern tropical areas which have an LAI of 2.0, and vegetation, rather than soil albedo, should have a larger influence. The northern tropical regions is also where the MODIS albedo used for evaluation had higher percentages of temporally fitted data which might also contribute to these biases.

Figure 5 shows that the implementation of the soil albedo scheme resulted in similar errors to the CNTL experiment for the Black and Blue-Sky VIS albedos, but large errors of up to −0.25 for the Black and Blue-Sky NIR albedos. These large errors were confined to central Australia (shown by the black box in the Black Sky NIR yearly panel), the most arid and dry part of the continent. The larger errors for the NIR as compared to the VIS albedos can be expected as NIR albedo is generally larger in magnitude as compared to VIS albedo. The fact that these errors are confined to the inland arid part suggests that the physical mechanisms leading to high albedo values in desert regions is not being adequately represented. Similar to CNTL, the PSALB experiment also showed larger errors during DJF (summer) as compared to the other seasons, noticeably in the northern tropical regions (also shown by a black box in the Black Sky NIR yearly panel). A monthly time series of the differences between PSALB and MODIS





GMDD
7, 1671–1707, 2014



over the central and northern areas is illustrated in Fig. 6, showing that PSALB consistently under-predicts the Black Sky NIR albedo during summer, whereas the errors in the central arid region show little monthly variation. The CNTL experiment showed similar consistent underestimation of Black Sky NIR albedo for the northern tropical region, suggesting that these errors are related to the parameterisation of vegetation, rather than soil albedo.

The soil albedo scheme implemented depends on soil colour, which is prescribed (Fig. 2c) and soil moisture. To better understand the uncertainties in the simulated soil moisture, we compared yearly and seasonal means of soil moisture from the CNTL experiment against AMSR-E satellite estimated surface soil moisture as shown in Fig. 7. CABLE soil moisture is generally higher as compared to AMSR-E for most of the continent. High soil moisture would result in lower simulated soil albedo and hence larger errors as compared to MODIS. However, these errors in soil moisture alone cannot explain the large errors of up to −0.25 in the centre of the continent. This is likely due to the known strong dependance of desert albedo on solar zenith angle, which is not explicitly represented in CABLE (Fig. 1).

Figure 8 shows the difference in overall albedo and surface fluxes between the PSALB and CNTL experiments (PSALB-CNTL). The lower albedo values in central Australia for the PSALB experiment result in an increase in net radiation of up to 45–50 $\mathrm{W\,m^{-2}}$, most of which increases sensible, rather than latent heat. This is expected for a semi-arid continent. The only noticeable change in latent heat is during the summer monsoon season (DJF) over the Northern tropical regions, when high precipitation leads to higher available soil water. Also illustrated in Fig. 8 is a diagnostic screen temperature showing the lower albedo and higher net radiation and sensible heat for the PSALB experiment lead to higher temperature by up to 0.5 °C. Such a change in temperature in not negligible, and implies that the new scheme should be used with caution.

To better understand the differences in the fluxes between the two experiments, we compared the simulated fluxes against the flux-tower observations. This is illustrated





GMDD
7, 1671–1707, 2014



in Fig. 9 showing a monthly times series of observed and simulated net radiation, sensible heat and latent heat flux at the Howard-Springs (HS) and Tumbarumba (TB) sites (Fig. 2b). Only the CNTL experiment is plotted as both simulations had very similar fluxes, as they are not located in regions where the differences between the CNTL and PSALB experiments were large. The RMSEs and biases for both simulations at both sites is summarised in Table 4, which shows only small differences between the two simulations. However, it is still useful to examine the performance of the model. CABLE systematically underestimates net radiation at the HS site, but performs remarkably well at the TB site. This may not be un-expected as the TB site experiences a temperate climate, with a clear seasonal cycle in the observed net radiation, whereas the HS site is close to the tropics and does not have such a clear seasonal signal. This systematic under prediction of net radiation could not be directly explained by the errors in albedo (Fig. 4).

## 4 Discussion

The CABLE land surface model prescribes background soil albedo and hence does not allow for soil moisture-albedo feedbacks, which the literature suggests can be important. To address this issue, we implemented a simple soil albedo scheme, based on soil moisture and colour, which has been commonly used in other LSMs. Two simulations were conducted, one with prescribed soil albedo derived from MODIS, the control (CNTL) experiment, and another with parameterised soil albedo (PSALB). The CNTL simulation showed relatively small errors in albedo when compared to MODIS whereas the PSALB experiment showed much larger errors especially in the VIS albedo. The differences were up to −0.25 and mainly in central Australia. The better performance of the CNTL as compared to PSALB is not surprising as the CNTL experiment uses a background soil albedo which is itself derived from earlier versions of MODIS albedo (Houldcroft et al., 2009). The large errors in the NIR albedo in the desert regions of Australia has been found elsewhere. Wang et al. (2004) compared albedo simulations





GMDD
7, 1671–1707, 2014



globally from the CLM2 LSM against MODIS and also found similar large errors in the NIR albedo in central Australia (see Fig. 5c in Wang et al., 2004). Numerous other studies have also found that the largest errors in NIR albedo from LSMs tend to be in desert and arid regions such as the Sahara (Wei et al., 2001; Oleson et al., 2003; Zhou et al., 2003; Wang et al., 2004). The much larger errors for the NIR as compared to the VIS albedo as found in this study has also been reported by Wang et al. (2004). This is due to the fact that NIR albedos over snow-free surfaces are larger in magnitude than the VIS albedo, and hence, likely to show larger error.

Given the large errors in albedo between MODIS and LSMs, Lawrence and Chase (2007) developed MODIS-consistent land-surface parameters, including the mapping of PFTs, LAI, and soil color for use within the CLM3 LSM. They clearly demonstrated that the use of the modified parameter maps improved surface albedo simulations when compared against MODIS albedo, which in some instances, resulted in improved simulations of precipitation and near-surface temperature. However the process of generating new soil colour maps involved the fitting of VIS and NIR albedos for each grid cell to reproduce values from MODIS, and then using the model soil moisture to re-compute corresponding soil colours. Hence, although a similar method could be applied using CABLE, this would lead to model-specific parameter mapping of a physical soil property for which there is no logical reason why it (soil colour) should be different across models. In the longer term, such an approach could lead to unnecessary complexity. Comparing the performance of models that have calibrated soil color adds a degree of unnecessary complexity that can be avoided by using observed soil color. The use of more accurate PFT maps however is more straight-forward, and examination of the MODIS MOD12C1 PFT yearly classification showed that the area of barren land in central Australia from 2001 to present is generally larger as compared to what is used for the simulations as shown in Fig. 2a. However, running CABLE with MOD12C1 yearly varying PFT maps (not shown) did not result in marked changes in albedo simulations as compared to MODIS.





GMDD
7, 1671–1707, 2014



The errors in albedo in central Australia are also likely due to inherent limitations of the parameterisation in Eq. (2), which was originally developed for the BATS LSM (Dickinson et al., 1993), adopted in CLM, and now in CABLE. Equation (2) is based on an absolute soil moisture value and this presents issues with regards to the universal application of the scheme irrespective of LSM, as the latter vary considerably in their treatment of soil moisture (Koster et al., 2009), as well as the processes which influence soil moisture (Koster and Milly, 1997). Specifically, the volumetric soil moisture simulated between LSMs is not transferable, rather it is a model-specific state that reflects the integration of many processes. These can be substantially avoided if future parameterisation are developed using soil wetness. This is a dimensionless index defined between extremes such as zero soil water, wilting point, field capacity, and saturation level, rather than soil moisture expressed as a volume of water. This issue is well known in the LSM community and was discussed in detail by Dirmeyer (2011). Another limitation is the 8 generic soil colour classes used, as well as the assumption that the ratio of the NIR to VIS albedo is exactly a factor of 2. However, Wang et al. (2005) have shown that this ratio from MODIS data over the arid part of central Australia is 2.69.

The cause of the large differences between LSM simulated and observed albedo in arid regions is the well established dependence of soil albedo on solar zenith angle (Wang et al., 2005; Yang et al., 2008), and the lack of explicit physical representation of this relationship in many LSMs. Wang et al. (2005) devised a semi-empirical scheme to relate bare soil albedo at a single site in the Sahel to solar zenith angle, and show improvements in albedo and surface flux simulations when applied to the NOAH land surface model. However, their simulations were at the site-scale, and over a very short time-frame (less than 2 months) and may not be easily applicable to regional or global simulations over longer time-frames. Liang et al. (2005) however, developed a so called “dynamic-statistical" parameterisation of snow-free albedo using MODIS albedo and soil moisture from a land data assimilation system over north America. Whilst the dynamical part of the model represents physical dependencies on solar zenith angle and





GMDD
7, 1671–1707, 2014



surface soil moisture etc., the statistical model provides parameter estimates specific to geographic location. This scheme has been shown to significantly improve albedo simulations in CLM over North America. A similar method could be adopted in CABLE in the future given we have identified this as a significant limitation of the model.

## 5 Conclusions

Surface albedo is a key element of the surface energy balance as it determines the amount of solar energy absorbed at the surface and re-distributed into sensible and latent heat, which in turn drive the surface energy and water cycles. In this study, we investigated how well CABLEv1.4b simulates albedo compared with MODIS estimates. We also tested a new simple parameterisation for the soil albedo, which is otherwise prescribed and held constant in time. This is an important step for the model as it enables the feedback between albedo and soil moisture to be represented. Our results show that CABLEv1.4b simulates overall albedo reasonably well when the soil albedo is prescribed as would be expected. The new parameterisation for soil albedo based on soil colour and soil moisture introduces large errors in the NIR albedo, especially in desert regions. These errors cannot be completely attributed to errors in soil moisture, or parameter uncertainties, but likely due to a lack of physical representation of zenith angle dependance of desert albedo. Hence, future development in CABLE albedo parameterisation should focus on incorporating this dependance and the work of Liang et al. (2005) provides a starting point in this direction. We also note that soil albedo parameterisations that use volumetric soil moisture, while entirely legitimate for the LSM they are designed for, are not easily transferable between LSMs. We recommend that future developments of soil albedo are based on the soil wetness, a quantity that is more transferable between models.





GMDD
7, 1671–1707, 2014



## Appendix A

### Parameterization of suface albedo in CABLEv1.4b

The overall albedo of the land surface ($\alpha_s$) is defined as:

$$\alpha_s = 0.5 \sum_{j=1,2} (\rho_{(\mathrm{dir},j)} f_b + \rho_{(\mathrm{dif},j)}(1 - f_b)) \quad \text{(A1)}$$

where $f_b$ is the fraction of direct beam shortwave radiation and $\rho_{(\mathrm{dir},j)}$ and $\rho_{(\mathrm{dif},j)}$ are the effective combined soil and canopy reflectance for direct and diffuse radiation in the VIS ($j = 1$) and NIR ($j = 2$) spectral bands.

The effective combined canopy reflectances ($\rho_{(\mathrm{dir},j)}$ and $\rho_{(\mathrm{dif},j)}$) in each band in Eq. (A1) are defined as:

$$\rho_{(\mathrm{dir},j)} = \rho_{(\mathrm{can\_dir},j)} + (\rho_{(\mathrm{soil},j)} - \rho_{(\mathrm{can\_dir},j)}) \exp(-2K^*_{(\mathrm{dir},j)}\Lambda) \quad \text{(A2)}$$

$$\rho_{(\mathrm{dif},j)} = \rho_{(\mathrm{can\_dif},j)} + (\rho_{(\mathrm{soil},j)} - \rho_{(\mathrm{can\_dif},j)}) \exp(-2K^*_{(\mathrm{dif},j)}\Lambda) \quad \text{(A3)}$$

where $\rho_{(\mathrm{can\_dir},j)}$ and $\rho_{(\mathrm{can\_dif},j)}$ is the canopy reflectance for direct and diffuse radiation, $\rho_{(\mathrm{soil},j)}$ is the soil reflectance, $K^*_{(\mathrm{dir},j)}$ and $K^*_{(\mathrm{dif},j)}$ are the extinction coefficients for direct and diffuse radiation, and $\Lambda$ the LAI.

The canopy direct and diffuse reflectance ($\rho_{(\mathrm{can\_dir},j)}$ and $\rho_{(\mathrm{can\_dif},j)}$) in each band in Eqs. (A2) and (A3) are defined as:

$$\rho_{(\mathrm{can\_dir},j)} = \frac{2K_{\mathrm{dir}}}{k_{\mathrm{dir}} + k_{\mathrm{dif}}} \rho_{(\mathrm{can\_black},j)} \quad \text{(A4)}$$

$$\rho_{(\mathrm{can\_dif},j)} = 2 \int_0^{\frac{\pi}{2}} \rho_{(\mathrm{can\_dir},j)} \sin(\theta)\cos(\theta)\mathrm{d}\theta \quad \text{(A5)}$$





GMDD
7, 1671–1707, 2014





where $K_{dir}$ and $K_{dif}$ are the extinctions coefficient for a canopy with black leaves for direct and diffuse radiation, $\rho_{(can\_black,j)}$ is the reflectance of a horizontally homogeneous canopy with horizontal black leaves, and $\theta$ is the solar zenith angle.

The extinction coefficients for a real canopy ($K^*_{dir}$ and $K^*_{dif}$) in Eqs. (A2) and (A3) and black canopy ($K_{dir}$ and $K_{dif}$) in Eqs. (A4) and (A5), are related as follows (Goudriaan and van Laar, 1994):

$$K^*_{(dir,j)} = k_{dir}(1-\omega_j)^{\frac{1}{2}}, \qquad K^*_{(dif,j)} = k_{dif}(1-\omega_j)^{\frac{1}{2}} \tag{A6}$$

where $\omega_j$ is the scattering coefficient for each waveband is equal to the sum of the canopy reflectance and transmittance.

The extinction coefficients for a black canopy ($K_{dir}$ and $K_{dif}$) in Eqs. (A4) and (A5) are defined as:

$$k_{dir}(\theta) = \frac{G}{\cos(\theta)} \tag{A7}$$

$$k_{dif} = -\frac{1}{\Lambda}\ln\left[\int_0^{\Lambda}\exp(-k_{direct}(\theta)\lambda)\mathrm{d}\lambda\right] \tag{A8}$$

where $\lambda$ is the cumulative canopy LAI from the canopy top and $G$ is the ratio of the projected area of leaves in the direction perpendicular to the direction of incident solar radiation and the actual leaf area:

$$G = \phi_1 + \phi_2\cos(\theta), \tag{A9}$$

$$\phi_1 = 0.5 - \chi(0.633 + 0.33\chi), \tag{A10}$$

$$\phi_2 = 0.877(1-2\phi_1) \tag{A11}$$

where $\chi$ is an empirical parameter related to the leaf angle distribution applicable over the range $[-0.4, 0.6]$.





GMDD
7, 1671–1707, 2014



Finally, the reflectance of a horizontally homogeneous canopy with horizontal black leaves ($\rho_{(\mathrm{can\_black},j)}$) in Eq. (A4) is defined as:

$$\rho_{(\mathrm{can\_black},j)} = \frac{1-(1-\omega_j)^{\frac{1}{2}}}{1+(1-\omega_j)^{\frac{1}{2}}} \tag{A12}$$

*Acknowledgements.* All the authors except David Mocko, Crystal B. Schaaf, and Qingsong Sun are supported by the Australian Research Council Centre of Excellence for Climate System Science (CE110001028). This work was also supported by the NSW Environment Trust (RM08603). We thank CSIRO and the Bureau of Meteorology through the Center for Australian Weather and Climate Research for their support in the use of the CABLE model. We thank the National Computational Infrastructure at the Australian National University, an initiative of the Australian Government, for access to supercomputer resources. We thank the NASA GSFC LIS team for support in coupling CABLE to LIS. The MODIS derived background soil albedo was provided by Peter R. J. North from the Department of Geography, Swansea University, Swansea, UK. The modified MODIS LAI data was provided by Hua Yuan from from the Land–Atmosphere Interaction Research Group at Beijing Normal University. This work used eddy covariance data acquired by the OzFlux FLUXNET community. The AMSR-E soil moisture data was provided by Yi Liu from the University of New South Wales. All of this assistance is gratefully acknowledged.

## References

Abramowitz, G., Leuning, R., Clark, M., and Pitman, A.: Evaluating the performance of land surface models, J. Climate, 21, 5468–5481, 2008. 1675, 1680

Avila, F. B., Pitman, A. J., Donat, M. G., Alexander, L. V., and Abramowitz, G.: Climate model simulated changes in temperature extremes due to land cover change, J. Geophys. Res., 117, D04108, doi:10.1029/2011JD016382 2012. 1679

Bonan, G.: Ecological Climatology, 2nd Edn., Cambridge University Press, 2008. 1673

Cruz, F. T., Pitman, A. J., and Wang, Y.-P.: Can the stomatal response to higher atmospheric carbon dioxide explain the unusual temperatures during the 2002 Murray-Darling Basin drought?, J. Geophys. Res., 115, D02101, doi:10.1029/2009JD012767, 2010. 1674





GMDD

7, 1671–1707, 2014



Davidson, A. and Wang, S.: The effects of sampling resolution on the surface albedos of dominant land cover types in the North American boreal region, Remote Sens. Environ., 93, 211–224, 2004. 1673

Decker, M., Pitman, A. J., and Evans, J. P.: Groundwater constraints on simulated transpiration variability over Southeastern Australian forests, J. Hydrometeorol., 14, 543–559, doi:10.1175/JHM-D-12-058.1 2012. 1678

Dickinson, R. E.: Land surface processes and climate-surface albedos and energy balance, Adv. Geophys., 25, 305–353, 1983. 1672

Dickinson, R. E., Henderson-Sellers, A., and Kennedy, P. J.: Biosphere–Atmosphere Transfer Scheme (BATS) Version 1e as coupled to the NCAR Community Model, NCAR Tech. Note, NCAR/TN-387+STR, 72 pp., Natl. Cent. Atmos. Res., Boulder, CO, 1993. 1677, 1685

Dickinson, R. E., Shaikh, M., Bryant, R., and Graumlich, L.: Interactive canopies for a climate model, J. Climate, 11, 2823–2836, 1998. 1675

Dirmeyer, P. A.: A history and review of the Global Soil Wetness Project (GSWP), J. Hydrometeorol., 12, 729–749, 2011. 1685

Exbrayat, J.-F., Pitman, A. J. J., Abramowitz, G., and Wang, Y.-P.: Sensitivity of net ecosystem exchange and heterotrophic respiration to parameterization uncertainty, J. Geophys. Res., 118, 1640–1651, doi:10.1029/2012JD018122, 2012. 1674

Goudriaan, J. and van Laar, H. H.: Modelling crop growth processes, Kluwer, Amsterdam, the Netherlands, 1994. 1688

Haverd, V., Raupach, M. R., Briggs, P. R., Canadell, J. G., Isaac, P., Pickett-Heaps, C., Roxburgh, S. H., van Gorsel, E., Viscarra Rossel, R. A., and Wang, Z.: Multiple observation types reduce uncertainty in Australia's terrestrial carbon and water cycles, Biogeosciences, 10, 2011–2040, doi:10.5194/bg-10-2011-2013, 2013. 1680

Hirsch, A. L., Kala, J., Pitman, A. J., Carouge, C., Evans, J. P., Haverd, V., and Mocko, D.: Impact of land surface initialisation approach on sub-seasonal forecast skill: a regional analysis in the Southern Hemisphere, J. Hydrometeorol., 15, 300–319, doi:10.1175/JHM-D-13-05.1, 2013. 1675

Houldcroft, C. J., Grey, W. M. F., Barnsley, M., Taylor, C. M., Los, S. O., and North, P. R. J.: New vegetation albedo parameters and global fields of soil background albedo derived from MODIS for use in a climate model, J. Hydrometeorol., 10, 183–198, 2009. 1678, 1683, 1700





GMDD
7, 1671–1707, 2014



Idso, S. B., Jackson, R. D., Reginato, R. J., Kimball, B. A., and Nakayama, F. S.: The dependence of bare soil albedo on soil water content, J. Appl. Meteorol., 14, 109–113, 1975. 1673, 1674

Jones, D., Wang, W., and Fawcett, R.: High-quality spatial climate data-sets for Australia, Aust. Meteorol. Mag., 58, 233–248, 2009. 1678

Kala, J., Decker, M., Exbrayat, J.-F., Pitman, A. J., Carouge, C., Evans, J. P., Abramowitz, G., and Mocko, D.: Influence of leaf area index prescriptions on simulations of heat, moisture, and carbon fluxes, J. Hydrometeorol., 15, 489–503, doi:10.1175/JHM-D-13-063.1, 2013. 1675

Keeling, C. D., Piper, S. C., Bacastow, R. B., Wahlen, M., Whorf, T. P., Heimann, M., and Meijer, H. A.: Atmospheric $CO_2$ and $^{13}CO_2$ exchange with the terrestrial biosphere and oceans from 1978 to 2000: observations and carbon cycle implications, in: A History of Atmospheric $CO_2$ and its effects on Plants, Animals, and Ecosystems, edited by: Ehleringer, J. R., Cerling, T. E., and Dearing, M. D., Springer Verlag, New York, 83–113, 2005. 1678

Koster, R. D. and Milly, P. C. D.: The interplay between transpiration and runoff formulations in land surface schemes used with atmospheric models, J. Climate, 10, 1578–1591, 1997. 1685

Koster, R. D., Guo, Z., Dirmeyer, P. A., Bonan, G., Chan, E., Cox, P., Davies, H., Gordon, C. T., Kanae, S., Kowalczyk, E., Lawrence, D., Liu, P., Lu, C.-H., Malyshev, S., McAveney, B., Mitchell, K., Mocko, D., Oki, T., Oleson, K. W., Pitman, A., Sud, Y. C., Taylor, C. M., Verseghy, D., Vasic, R., Xue, Y., and Yamada, T.: Regions of strong coupling between soil moisture and precipitation, Science, 305, 1138–1140, 2004. 1673

Koster, R. D., Guo, Z., Yang, R., Dirmeyer, P. A., Mitchell, K., and Puma, M. J.: On the nature of soil moisture in land surface models, J. Climate, 22, 4322–4335, 2009. 1685

Kowalczyk, E. A., Wang, Y. P., Law, R. M., Davies, H. L., McGregor, J. L., and Abramowitz, G.: The CSIRO Atmosphere Biosphere Land Exchange model for use in climate models and as an offline model, Commonwealth Scientific and Industrial Research Organisation Marine and Atmospheric Research Paper 013, November 2006, available online: www.cmar.csiro.au/e-print/open/kowalczykea_2006a.pdf (last access: 10 November 2011), 37 pp., 2006. 1675

Kumar, S., Peters-Lidard, C., Tian, Y., Houser, P., Geiger, J., Olden, S., Lighty, L., Eastman, J., Doty, B., Dirmeyer, P., Adams, J., Mitchell, K., Wood, E., and Sheffield, J.: Land information system: an interoperable framework for high resolution land surface modeling, Environ. Modell. Softw., 21, 1402–1415, 2006. 1677





GMDD
7, 1671–1707, 2014



Kumar, S. V., Peters-Lidard, C. D., Eastman, J. L., and Tao, W.-K.: An integrated high-resolution hydrometeorological modeling testbed using LIS and WRF, Environ. Modell. Softw., 23, 169–181, 2008. 1677

Lawrence, P. J. and Chase, T. N.: Representing a new MODIS consistent land surface in the Community Land Model (CLM 3.0), J. Geophys. Res.-Biogeo., 112, G01023, doi:10.1029/2006JG000168, 2007. 1674, 1684

Liang, X.-Z., Xu, M., Gao, W., Kunkel, K., Slusser, J., Dai, Y., Min, Q., Houser, P. R., Rodell, M., Schaaf, C. B., and Gao, F.: Development of land surface albedo parameterization based on Moderate Resolution Imaging Spectroradiometer (MODIS) data, J. Geophys. Res.-Atmos., 110, D11107, doi:10.1029/2004JD005579, 2005. 1674, 1685, 1686

Liu, Y. Y., van Dijk, A. I. J. M., de Jeu, R. A. M., and Holmes, T. R. H.: An analysis of spatiotemporal variations of soil and vegetation moisture from a 29-year satellite-derived data set over mainland Australia, Water Resour. Res., 45, W07405, doi:10.1029/2008WR007187, 2009. 1680

Lucht, W., Schaaf, C., and Strahler, A.: An algorithm for the retrieval of albedo from space using semi-empirical BRDF models, IEEE T. Geosci. Remote, 38, 977–998, 2000. 1679

Mao, J., Phipps, S. J., Pitman, A. J., Wang, Y. P., Abramowitz, G., and Pak, B.: The CSIRO Mk3L climate system model v1.0 coupled to the CABLE land surface scheme v1.4b: evaluation of the control climatology, Geosci. Model Dev., 4, 1115–1131, doi:10.5194/gmd-4-1115-2011, 2011. 1675

Meng, X., Evans, J., and McCabe, M.: The influence of inter-annually varying albedo on regional climate and drought, Clim. Dynam., 42, 787–803, doi:10.1007/s00382-013-1790-0, 2013. 1674

Oleson, K. W., Bonan, G. B., Schaaf, C., Gao, F., Jin, Y., and Strahler, A.: Assessment of global climate model land surface albedo using MODIS data, Geophys. Res. Lett., 30, 1443, doi:10.1029/2002GL0167498, 2003. 1674, 1679, 1684

Pitman, A. J., Avila, F. B., Abramowitz, G., Wang, Y. P., Phipps, S. J., and de Noblet-Ducoudré, N.: Importance of background climate in determining impact of land-cover change on regional climate, Nature Climate Change, 9, 472–475, 2011. 1674, 1679

Raupach, M. R.: Simplified expressions for vegetation roughness length and zero-plane displacement as functions of canopy height and area index, Bound.-Lay. Meteorol., 71, 211–216, 1994. 1675





GMDD
7, 1671–1707, 2014



Rienecker, M. M., Suarez, M. J., Gelaro, R., Todling, R., Bacmeister, J., Liu, E., Bosilovich, M. G., Schubert, S. D., Takacs, L., Kim, G.-K., Bloom, S., Chen, J., Collins, D., Conaty, A., da Silva, A., Gu, W., Joiner, J., Koster, R. D., Lucchesi, R., Molod, A., Owens, T., Pawson, S., Pegion, P., Redder, C. R., Reichle, R., Robertson, F. R., Ruddick, A. G., Sienkiewicz, M., and Woollen, J.: MERRA: NASA's Modern-Era Retrospective Analysis for Research and Applications, J. Climate, 24, 3624–3648, 2011. 1678

Schaaf, C. B., Gao, F., Strahler, A. H., Lucht, W., Li, X., Tsang, T., Strugnell, N. C., Zhang, X., Jin, Y., Muller, J.-P., Lewis, P., Barnsley, M., Hobson, P., Disney, M., Roberts, G., Dunderdale, M., Doll, C., d'Entremont, R. P., Hu, B., Liang, S., Privette, J. L., and Roy, D.: First operational BRDF, albedo nadir reflectance products from MODIS, Remote Sens. Environ., 83, 135–148, 2002. 1679

Spitters, C.: Separating the diffuse and direct component of global radiation and its implications for modeling canopy photosynthesis Part II. Calculation of canopy photosynthesis, Agr. Forest Meteorol., 38, 231–242, 1986. 1676

Tsvetsinskaya, E. A., Schaaf, C. B., Gao, F., Strahler, A. H., Dickinson, R. E., Zeng, X., and Lucht, W.: Relating MODIS-derived surface albedo to soils and rock types over Northern Africa and the Arabian peninsula, Geophys. Res. Lett., 29, D20106, doi:10.1029/2005JD006772, 2002. 1677

Vamborg, F. S. E., Brovkin, V., and Claussen, M.: The effect of a dynamic background albedo scheme on Sahel/Sahara precipitation during the mid-Holocene, Clim. Past, 7, 117–131, doi:10.5194/cp-7-117-2011, 2011. 1677

Wang, Y.-P. and Leuning, R.: A two-leaf model for canopy conductance, photosynthesis and partitioning of available energy I: Model description and comparison with a multi-layered model, Agr. Forest Meteorol., 91, 89–111, 1998. 1675

Wang, Y. P., Kowalczyk, E., Leuning, R., Abramowitz, G., Raupach, M. R., Pak, B., van Gorsel, E., and Luhar, A.: Diagnosing errors in a land surface model (CABLE) in the time and frequency domains, J. Geophys. Res., 116, G01034, doi:10.1029/2010JG001385, 2011. 1674, 1675

Wang, Y. P., Lu, X. J., Wright, I. J., Dai, Y. J., Rayner, P. J., and Reich, P. B.: Correlations among leaf traits provide a significant constraint on the estimate of global gross primary production, Geophys. Res. Lett., 39, L19405, doi:10.1029/2012GL053461, 2012. 1674





GMDD
7, 1671–1707, 2014



Wang, Z., Zeng, X., Barlage, M., Dickinson, R. E., Gao, F., and Schaaf, C. B.: Using MODIS BRDF and albedo data to evaluate global model land surface albedo, J. Hydrometeorol., 5, 3–14, 2004. 1674, 1677, 1679, 1683, 1684

Wang, Z., Barlage, M., Zeng, X., Dickinson, R. E., and Schaaf, C. B.: The solar zenith angle dependence of desert albedo, Geophys. Res. Lett., 32, L05403, doi:10.1029/2004GL021835, 2005. 1674, 1685

Wang, Z., Schaaf, C. B., Strahler, A. H., Chopping, M. J., Roman, M. O., Shuai, Y., Woodcock, C. E., Hollinger, D. Y., and Fitzjarrald, D. R.: Evaluation of MODIS albedo product (MCD43A) over grassland, agriculture and forest surface types during dormant and snow-covered periods, Remote Sens. Environ., 140, 60–77, 2014. 1679

Wei, X., Hahmann, A. N., Dickinson, R. E., Yang, Z.-L., Zeng, X., Schaudt, K. J., Schaaf, C. B., and Strugnell, N.: Comparison of albedos computed by land surface models and evaluation against remotely sensed data, J. Geophys. Res.-Atmos., 106, 20687–20702, 2001. 1674, 1684

Yang, F., Mitchell, K., Hou, Y.-T., Dai, Y., Zeng, X., Wang, Z., and Liang, X.-Z.: Dependence of land surface albedo on solar zenith angle: observations and model parameterization, J. Appl. Meteorol. Clim., 47, 2963–2982, 2008. 1674, 1685

Yuan, H., Dai, Y., Xiao, Z., Ji, D., and Shangguan, W.: Reprocessing the MODIS Leaf Area Index products for land surface and climate modelling, Remote Sens. Environ., 115, 1171–1187, 2011. 1678, 1701

Zaitchik, B. F., Santanello, J. A., Kumar, S. V., and Peters-Lidard, C. D.: Representation of soil moisture feedbacks during drought in NASA Unified WRF (NU-WRF), J. Hydrometeorol., 14, 360–367, doi:10.1175/JHM-D-12-069.1, 2012. 1674, 1677

Zeng, X., Shaikh, M., Dai, Y., Dickinson, R. E., and Myneni, R.: Coupling of the Common Land Model to the NCAR Community Climate Model, J. Climate, 15, 1832–1854, 2002. 1677

Zhang, Q., Wang, Y. P., Pitman, A. J., and Dai, Y. J.: Limitations of nitrogen and phosphorous on the terrestrial carbon uptake in the 20th century, Geophys. Res. Lett., 38, L22701, doi:10.1029/2011GL049244, 2011. 1674

Zhou, L., Dickinson, R. E., Tian, Y., Zeng, X., Dai, Y., Yang, Z.-L., Schaaf, C. B., Gao, F., Jin, Y., Strahler, A., Myneni, R. B., Yu, H., Wu, W., and Shaikh, M.: Comparison of seasonal and spatial variations of albedos from Moderate-Resolution Imaging Spectroradiometer (MODIS) and Common Land Model, J. Geophys. Res.-Atmos., 108, 4488, doi:10.1029/2002JD003326, 2003. 1674, 1679, 1684





GMDD
7, 1671–1707, 2014



**Table 1.** Names of plant functional types (PFTs) and soil types shown in Fig. 2a.

| PFT number | PFT |
|---|---|
| 1 | Evergreen Needleleaf |
| 2 | Evergreen Broadleaf |
| 3 | Deciduous Needleleaf |
| 4 | Deciduous Broadleaf |
| 5 | Mixed Forest |
| 6 | Closed Shrublands |
| 7 | Open Shrublands |
| 8 | Woody Savannas |
| 9 | Savannas |
| 10 | Grasslands |
| 11 | Permanent Wetlands |
| 12 | Croplands |
| 13 | Urban and Built-up |
| 14 | Cropland Mosaics |
| 15 | Snow and Ice |
| 16 | Barren |





GMDD
7, 1671–1707, 2014



**Table 2.** Saturated and dry soil albedos for different soil colours (Fig. 2c) in the VIS and NIR wavebands.

| Soil Color | $\alpha_{sat}$ NIR | $\alpha_{sat}$ VIS | $\alpha_{dry}$ NIR | $\alpha_{dry}$ VIS |
|---|---|---|---|---|
| 1 | 0.12 | 0.24 | 0.24 | 0.48 |
| 2 | 0.11 | 0.22 | 0.22 | 0.44 |
| 3 | 0.10 | 0.20 | 0.20 | 0.40 |
| 4 | 0.09 | 0.18 | 0.18 | 0.36 |
| 5 | 0.08 | 0.16 | 0.16 | 0.32 |
| 6 | 0.07 | 0.14 | 0.14 | 0.28 |
| 7 | 0.06 | 0.12 | 0.12 | 0.24 |
| 8 | 0.05 | 0.10 | 0.10 | 0.20 |





GMDD
7, 1671–1707, 2014



**Table 3.** Root-mean-square error (RMSE) and bias (scaled by 100) between the CNTL and PSALB experiments and MODIS black-sky (Black-S) and blue-sky (Blue-S) visible (VIS) and near infra-red (NIR) albedo at the yearly and seasonal time-scale.

| | YEARLY | | DJF | | MAM | | JJA | | SON | |
|---|---|---|---|---|---|---|---|---|---|---|
| | RMSE | Bias | RMSE | Bias | RMSE | Bias | RMSE | Bias | RMSE | Bias |
| CNTL | | | | | | | | | | |
| Black-S-VIS | 3.43 | 2.40 | 2.71 | 1.13 | 3.80 | 2.80 | 4.28 | 3.36 | 3.37 | 2.30 |
| Black-S-NIR | 7.18 | −6.06 | 8.85 | −7.86 | 7.11 | −5.91 | 6.45 | −4.97 | 6.72 | −5.52 |
| Blue-S-VIS | 6.75 | 6.30 | 6.17 | 5.63 | 6.94 | 6.53 | 7.53 | 7.11 | 6.43 | 5.91 |
| Blue-S-NIR | 3.52 | 2.10 | 3.53 | 1.88 | 3.54 | 1.97 | 3.99 | 2.60 | 3.37 | 1.94 |
| PSALB | | | | | | | | | | |
| Black-S-VIS | 3.40 | 0.64 | 3.37 | −0.59 | 3.59 | 0.99 | 3.85 | 1.66 | 3.43 | 0.50 |
| Black-S-NIR | 9.47 | −7.65 | 10.96 | −9.38 | 9.44 | −7.58 | 8.75 | −6.54 | 9.08 | −7.12 |
| Blue-S-VIS | 4.83 | 3.56 | 4.27 | 2.74 | 5.02 | 3.79 | 5.57 | 4.51 | 4.66 | 3.21 |
| Blue-S-NIR | 5.48 | −0.45 | 5.56 | −0.80 | 5.60 | −0.61 | 5.61 | 0.15 | 5.42 | −0.54 |





GMDD
7, 1671–1707, 2014



**Table 4.** Root-mean-square error (RMSE) and bias ($W m^{-2}$) in net radiation (Rnet), sensible heat flux (Qh), and latent heat flux (Qle) at the Howard Springs and Tumbarumba FLUXNET stations (Fig. 2b) for the CNTL and PSALB experiment.

| | CNTL | | | | PSALB | | | |
|---|---|---|---|---|---|---|---|---|
| | Howard springs | | Tumbarumba | | Howard springs | | Tumbarumba | |
| Flux | RMSE | Bias | RMSE | Bias | RMSE | Bias | RMSE | Bias |
| Rnet | 28.3 | −20.0 | 15.3 | 4.5 | 30.7 | −23.5 | 15.3 | 4.4 |
| Qh | 26.5 | 5.6 | 24.8 | −0.1 | 24.1 | 2.3 | 24.8 | −0.1 |
| Qle | 26.7 | −13.9 | 26.9 | −5.0 | 26.7 | −14.2 | 26.9 | −5.0 |





GMDD
7, 1671–1707, 2014





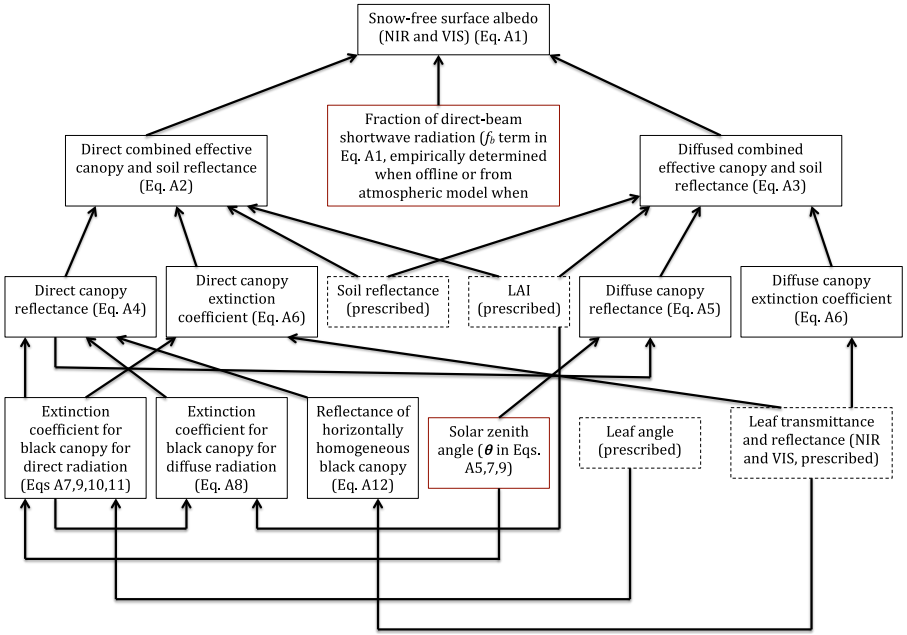


**Fig. 1.** Schematic illustration of snow-free surface albedo parameterisation in CABLE. Boxes with dashed lines represent user-defined input parameters to the model. The boxes with solid black lines represent the equations described in Appendix A and the boxes in solid red lines represent terms used in the equations.





GMDD
7, 1671–1707, 2014



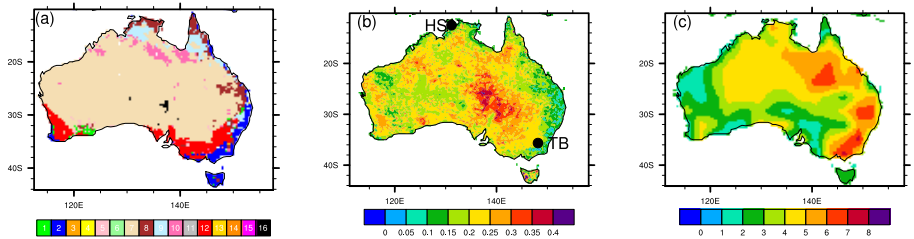


**Fig. 2. (a)** Distribution of PFTs in the domain, **(b)** prescribed background snow-free soil albedo from Houldcroft et al. (2009) used in the CNTL experiment, and **(c)** soil colours used in the PSALB experiment. The black dots in panel **(b)** represent the station location of the Howard-Springs (HS) and Tumbarumba (TB) FLUXNET sites described in Sect. 2.4. The PFTs in panel **(a)** are shown in Table 1.





GMDD
7, 1671–1707, 2014



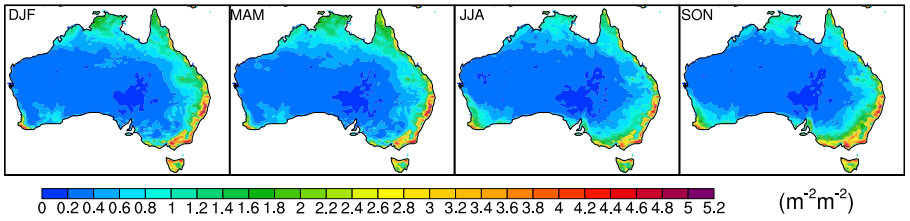


**Fig. 3.** Seasonal mean LAI from Yuan et al. (2011) (monthly means are used in the simulations).





GMDD
7, 1671–1707, 2014



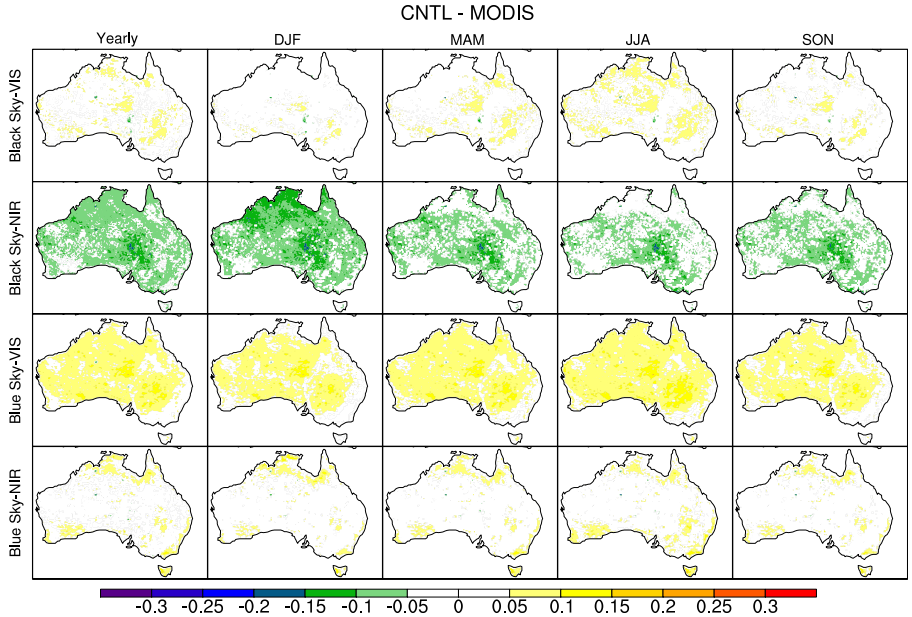


**Fig. 4.** Mean yearly and seasonal differences between CNTL and MODIS albedo (CNTL-MODIS) over the period 2001–2008. December-January-February (DJF) is summer, March-April-May (MAM) is autumn, June-July-August (JJA) is winter, September-October-November (SON) is spring.





GMDD
7, 1671–1707, 2014



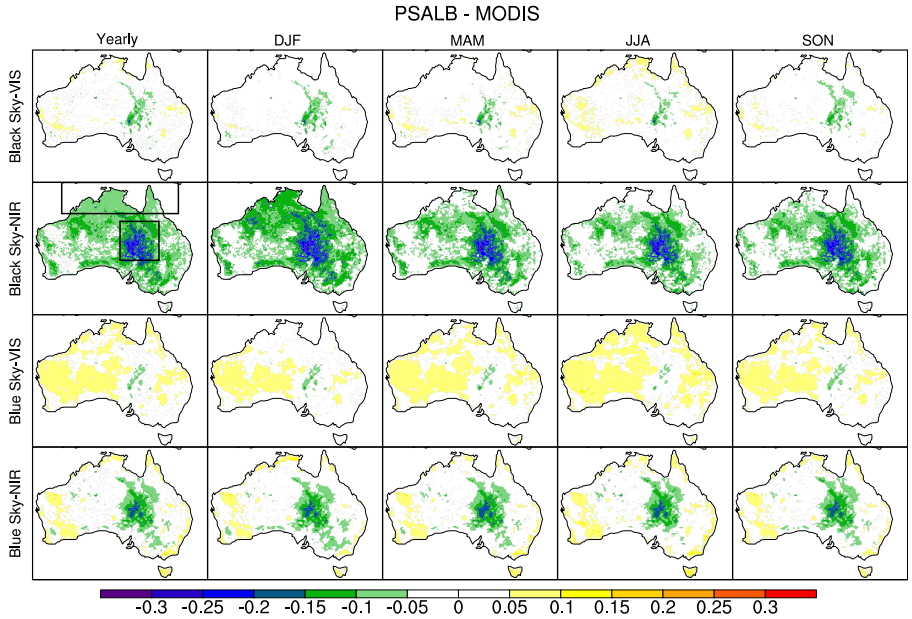


**Fig. 5.** Same as in Fig. 4, except for the PSALB experiment (PSALB-MODIS). The northern and central boxes in the Black Sky-NIR yearly panel show the regions from which a time-series is plotted in Fig. 6.





GMDD
7, 1671–1707, 2014



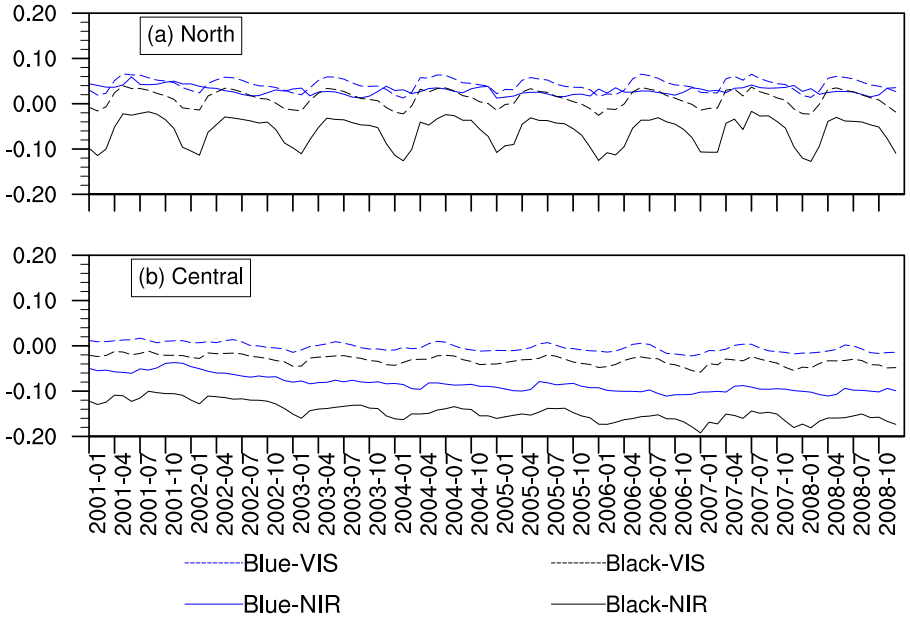


**Fig. 6.** Monthly time series of difference between PSALB and MODIS (PSALB-MODIS) spatially averaged over the northern and central boxes shown in the Black Sky-NIR yearly panel in Fig. 5.





GMDD
7, 1671–1707, 2014



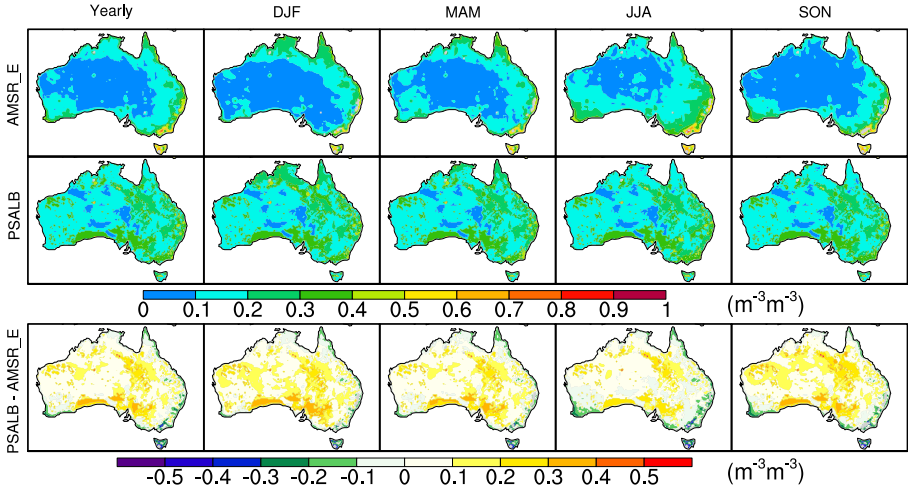


**Fig. 7.** Yearly and seasonal soil moisture from AMSR-E, the PSALB experiment, and difference between PSALB and AMSR-E (PSALB-AMSR_E).





GMDD
7, 1671–1707, 2014



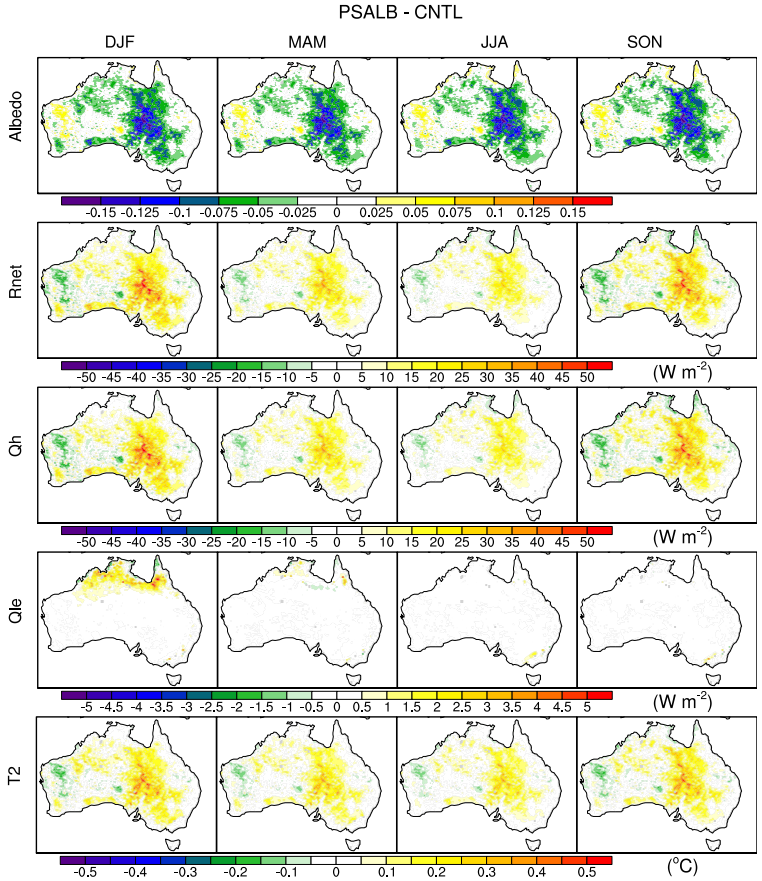


**Fig. 8.** Seasonal differences in albedo, net radiation (Rnet), sensible heat (Qh), latent heat (Qle) flux and screen level derived temperature (T2) between the PSALB and CNTL experiments (PSALB-CNTL).





GMDD
7, 1671–1707, 2014



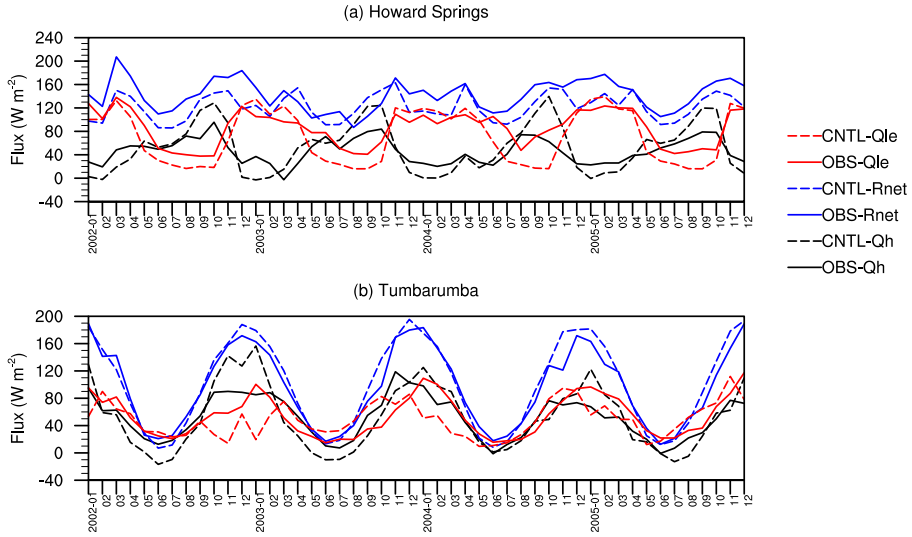


**Fig. 9.** Time series of mean monthly observed (solid lines) and CNTL (dotted lines) net radiation (blue), sensible heat flux (black), and latent heat flux (red) at **(a)** the Howard Springs, and **(b)** Tumbarumba sites (Fig. 2b).





GMDD
7, 1671–1707, 2014